PCCP

PAPER

Cite this: *Phys. Chem. Chem. Phys.*, 2018, **20**, 21739

Received 24th June 2018,
Accepted 9th August 2018

DOI: 10.1039/c8cp04007a

rsc.li/pccp

Dissociative electron attachment to $HGaF_4$ Lewis–Brønsted superacid

Marcin Czapla,[a] Jack Simons[b] and Piotr Skurski*[ab]

The consequences of an excess electron attachment to $HGaF_4$ (HF/GaF_3) superacid are investigated on the basis of theoretical calculations employing *ab initio* methods. It is found that the dipole potential of $HGaF_4$ plays an important role in the initial formation of a dipole-bound anionic state. Due to the kinetic instability of that initially formed anion, a fragmentation reaction occurs promptly and leads to $(GaF_4)^-$ and H as the final products. The energy profile of this process, its rate, and mechanism are presented and discussed.

1. Introduction

It is commonly known that attaching an excess electron to a molecule might result in its fragmentation. For example, in electron capture dissociation[1,2] or electron transfer dissociation[3,4] an electron is initially attached mostly to a positively charged site within the gas-phase sample, which is followed by the cleavage of various bonds. In consequence, characteristic fragmentation products are generated; however, the mechanism of their formation remains uncertain in many cases. Recently, we considered the possibility of forming a negatively charged anionic state of $HAlF_4$ and stumbled across its instability induced by an excess electron attachment (as it turned out that $(HAlF_4)^-$ is not geometrically stable and spontaneously detaches a hydrogen atom to produce the $(AlF_4)^-$ anion).[5] Hence, our findings indicated that certain superacids might be susceptible to fragmentation induced by zero-kinetic energy excess electron attachment. Namely, the $HAlF_4$ molecule (chosen as a representative superacid[6–12]) was found capable of an excess electron binding due to its dipole potential. However, the resulting (*i.e.*, initially formed) anionic state of dipole-bound nature ($HAlF_4^-$), although electronically bound, turned out to be kinetically unstable. In particular, the $HAlF_4^-$ system was found to undergo an immediate structural reorganization driven by the $(AlF_4)^-$ strongly-bound superhalogen[13–28] anion formation. The potential energy surface analysis led to the conclusion that the $(HAlF_4)^- \rightarrow (AlF_4)^- + H$ transformation should proceed spontaneously and involve the simultaneous structure relaxation of the AlF_4 moiety (in the direction allowing it to approach tetrahedral geometry) and the excess electron density migration from the area outside the molecular framework to the valence AlF_4 region. The fragmentation of the $HAlF_4$ superacid molecule was predicted to be the final effect of the excess electron attachment process. These recent results revealed not only the important role of the initially formed $(HAlF_4)^-$ dipole-bound anionic state of the $HAlF_4$ superacid but also indicated the possible superacids' susceptibility to dissociative electron attachment (DEA). Due to many potential applications[29,30] of this phenomenon it seems important to investigate the DEA processes with respect to superacids in greater detail.

Hence, in this work we focus on (i) providing the energy balance concerning the representative superacid + e^- → superhalogen$^-$ + H process, and (ii) evaluating the rate of the subsequent fragmentation of the superacid anion. We have chosen to illustrate these phenomena by studying the $HGaF_4$ binary Lewis–Brønsted superacid whose properties are believed to be similar to those of other superacid molecules consisting of a (Lewis acid)/(Brønsted acid) pair connected to each other *via* the dative bond.

2. Methods

The equilibrium structures and the corresponding harmonic vibrational frequencies for the stationary points on the potential energy surface were calculated using the second-order Møller–Plesset (MP2) perturbational method whereas the electron binding energy of the initially formed $(HGaF_4)^-$ anionic state was evaluated using the coupled-cluster method with single, double, and non-iterative triple excitations (CCSD(T)).[31,32] The relaxed scan of the ground doublet state $(HGaF_4)^-$ anionic potential energy surface was performed using the MP2 method.

Since we used the methods based on an unrestricted Hartree–Fock (UHF) starting point it was important to make sure that little

[a] *Laboratory of Quantum Chemistry, Faculty of Chemistry, University of Gdańsk, Wita Stwosza 63, Gdańsk 80-308, Poland. E-mail: piotr.skurski@ug.edu.pl*
[b] *Henry Eyring Center for Theoretical Chemistry, Department of Chemistry, University of Utah, Salt Lake City, UT 84112, USA*

(if any) spin contamination enters into the final wave functions. We computed the expectation value $\langle S^2 \rangle$ for the states studied in this work and found values not exceeding 0.7524 in doublet anionic cases (at the UHF level). Hence we are confident that spin contamination is not large enough to significantly affect our findings.

As far as the basis sets are concerned, we decided to use the aug-cc-pVTZ basis[33] supplemented with additional 4s4p3d sets of diffuse functions. Our choice was dictated by the necessity of employing the basis set which is appropriate for both weakly dipole-bound anion and strongly valence-bound superhalogen anion. Therefore, in order to properly describe the neutral molecular host, the aug-cc-pVTZ basis set was chosen, as its usefulness in describing dipole-bound anions was demonstrated in the past and compared to other commonly used one-electron basis sets.[34] Since the aug-cc-pVTZ basis set was also found to be adequate for describing the equilibrium structures and electronic stabilities of strongly bound superhalogen anions,[35] our choice seems appropriate. However, the diffuse character of the orbital describing the loosely bound electron (in a dipole-bound anionic state) necessitates the use of extra diffuse basis functions having very low exponents. Albeit we do realize that such an additional set of diffuse functions is not necessary to describe the strongly bound valence anionic state formed as the product of the process investigated, it is required to properly describe the dipole-bound anionic state that is initially formed during this process. Hence, while studying the properties of that initially formed dipole-bound anionic state of the $HGaF_4$ acid we performed the calculations using the aug-cc-pVTZ basis set[33] supplemented with an additional 4s4p3d set of diffuse functions centered on the hydrogen atom. The calculations for the remaining neutral and anionic states described in this work (including those examined while performing the relaxed potential energy surface scan) were carried out using the same aug-cc-pVTZ + 4s4p3d basis set in order to maintain consistency.

We verified that the inclusion of one additional diffuse 1s1p1d set (which led to the aug-cc-pVTZ + 5s5p4d basis set) increases the vertical electron binding energy of the dipole-bound $(HGaF_4)^-$ anionic state by less than 1 cm^{-1} (when calculated at the MP2 level) hence we are confident that the use of the aug-cc-pVTZ basis set with the additional 4s4p3d is sufficient for estimating the electronic stabilities of the weakly bound anionic states investigated.

The extra diffuse functions do not share exponent values and we used even-tempered[36] four-term s, four-term p, and three-term d basis sets. The geometric progression ratio was equal to 5.0[34], and for each symmetry we started to build up the exponents of the extra diffuse functions from the lowest exponent of the same symmetry included in the aug-cc-pVTZ basis set designed for hydrogen. As a consequence, we achieved the lowest exponents of 4.0416×10^{-5}, 1.6320×10^{-4}, and 1.9760×10^{-3} a.u., for the s, p, and d symmetries, respectively.

The partial atomic charges were fitted to the electrostatic potential according to the Merz–Singh–Kollman scheme.[37]

All calculations were performed with the Gaussian09 (Rev.D.01) software package.[38] In order to avoid erroneous results from the default direct SCF calculations with the basis sets with large s, p, and d sets of diffuse functions, the keyword SCF = NoVarAcc was used and the two-electron integrals were evaluated (without prescreening) to a tolerance of 10^{-20} a.u.

3. Results and discussion

3.1. Formation of the $(HGaF_4)^-$ dipole-bound anion

Since the $(HGaF_4)^-$ anion is assumed to be formed by an excess electron attachment to the $HGaF_4$ system, the equilibrium structure of that neutral parent molecule seems important for our investigation. In fact, the lowest energy structure of the $HGaF_4$ superacid was described earlier[9] as consisting of two interacting fragments (GaF_3 and HF) held together by a HF → GaF_3 dative bond (involving the fluorine of HF electron lone pair and the 4p empty orbital of Ga) and a $GaF_3 \cdots HF$ hydrogen bond. In order to assure consistency, we reexamined the equilibrium structure of $HGaF_4$ by employing the MP2/aug-cc-pVTZ + 4s4p3d level and found that the geometrical parameters obtained are very similar to those reported earlier (the differences in bond lengths and valence angles do not exceed 0.119 Å and 6°, respectively).[9]

We verified that the $HGaF_4$ molecule cannot support a bound valence anionic state, hence the only possibility to attach an excess electron derives from the dipole potential. The polarity of $HGaF_4$ manifests itself by the dipole moment of 3.091 Debye, as calculated for the C_s-symmetry equilibrium structure of the neutral species using the HF electron densities (the calculations utilizing the MP2 and QCISD densities led to similar values of 2.979 and 2.976 D, respectively). Such a dipole moment is large enough to bind an extra electron (the polarity of the corresponding neutral molecule should be larger than 2.5 Debye to support a dipole-bound anionic state[39]), hence one may expect $HGaF_4$ to form an electronically stable anion. As established by many previous studies,[40–49] the excess electron density in a dipole-bound anion is diffuse and localized outside the molecular framework.

The distribution of the excess electron density in the case of the $(HGaF_4)^-$ anion follows that pattern as the singly occupied molecular orbital (SOMO) holding an extra electron resembles the typical SOMOs predicted for many other dipole-bound anions.[50–52] The vertical electron attachment energy (VAE) predicted for the $(HGaF_4)^-$ anion equals to 1451 cm^{-1} (as calculated at the CCSD(T)/aug-cc-pVTZ + 4s4p3d level) and this value is similar to that found for the $(HAlF_4)^-$ anion (1106 cm^{-1}) whose neutral parent $HAlF_4$ exhibits polarity comparable to the neutral $HGaF_4$.[5] The excess electron binding energy determined for $(HGaF_4)^-$ at the Hartree–Fock level (at which only the electrostatic, exchange and induction interactions are taken into account) is only 85 cm^{-1}, which indicates that the electron correlation effects are responsible for *ca.* 94% of the VAE. Even though such a large contribution coming from electron correlation effects might seem surprising, it is a common feature of many other dipole-bound anions studied in the past. It should also be noted that we provide neither the vertical electron detachment energy of

the $(HGaF_4)^-$ anion nor the adiabatic electron affinity of the $HGaF_4$ neutral molecule because our calculations indicated that $(HGaF_4)^-$ is not geometrically stable (see the following section), thus these two quantities cannot be evaluated.

3.2. Fragmentation of $(HGaF_4)^-$

As it was mentioned in the preceding section, the $(HGaF_4)^-$ anion is not geometrically stable. Once an excess electron is attracted by the dipole potential of the neutral polar $HGaF_4$ molecule to form the dipole-bound species, it penetrates its valence region and the whole $(HGaF_4)^-$ structure undergoes a significant reorganization. This means that, unlike the majority of other dipole-bound anions described thus far (for which only minor geometry relaxation upon excess electron attachment was observed), but similar to the $(HAlF_4)^-$ anion reported recently,[5] significant structure relaxation in the case of $(HGaF_4)^-$ is predicted. In fact, this reorganization is associated with the evolution of the excess electron density distribution that finally leads to the hydrogen atom loss and the $(GaF_4)^-$ anion formation.

In Fig. 1 (see also Table 1) we present the energy profile for the $(HGaF_4)^-$ anion obtained by performing a relaxed scan of the ground doublet electronic state potential energy surface along the coordinate corresponding to the distance between the F atom and the departing H atom (the SOMOs for the arbitrarily chosen structures are also depicted). Having this energy profile at hand, we can discuss the fragmentation of $HGaF_4$ caused by an excess electron attachment. We would like to stress that we consider the initial formation of the $(HGaF_4)^-$ dipole-bound anion as a crucial step in the whole process as the neutral $HGaF_4$ superacid molecule has no other way of attracting a distant excess electron but through its dipole potential which plays an attractor role. In other words, the dipole potential of the neutral $HGaF_4$ molecule enables the long-range attraction of an extra electron, which leads to the formation of a short-lived dipole-bound anionic state. This initial step opens the door to further processes that follow, including the electron density evolution, structure relaxation, and finally the H–F bond homolytic cleavage.

Table 1 The r(H–F) and r(Ga–FH) distances (in Å), the F–Ga–F–F dihedral angles δ (in degrees) and the relative energies RE (in kcal mol^{-1}) characterizing the data points plotted in Fig. 1. The vertical electron detachment energies (VDE) at each geometry are given in eV. The last row (r(H–F) = ∞) corresponds to the isolated $(GaF_4)^-$ anion at its equilibrium T_d-symmetry structure[53,54]

r(H–F)	r(Ga–FH)	δ	RE	VDE
0.939	2.059	159.77	32.8	0.18
1.000	1.942	129.42	22.5	1.05
1.200	1.858	125.16	18.3	2.34
1.400	1.819	122.95	11.8	3.98
1.600	1.803	121.81	6.4	5.43
1.800	1.794	121.17	3.1	6.66
2.000	1.790	120.76	1.3	7.49
2.200	1.788	120.50	0.5	8.07
2.400	1.787	120.35	0.1	8.45
2.600	1.786	120.25	<0.1	8.50
2.655	1.786	120.23	0.0	8.42
2.800	1.786	120.19	<0.1	8.94
3.000	1.786	120.25	0.1	9.05
4.000	1.785	120.05	0.4	9.01
5.000	1.785	120.03	0.6	9.15
∞	1.785	120.00	0.9	9.10

The SOMO for the r(H–F) = 0.939 Å in Fig. 1 corresponds to the singly occupied orbital holding an excess electron in the initially formed $(HGaF_4)^-$ dipole-bound anion. The fraction of electron density included inside each orbital is the following: 20% (r = 0.939 Å), 94% (r = 1.2 Å), 94% (r = 1.6 Å), 98% (r = 2.655 Å), 98% (r = 3.0 Å), and 98% (r = 5.0 Å) (note that the dipole orbital for r = 0.939 Å would be significantly larger if plotted with the consistent contour value; its size had to be reduced to fit the picture). As explained above, this orbital is diffuse and localized outside the molecular framework (in the vicinity of the positive pole of the molecular dipole). The absence of any (even shallow)

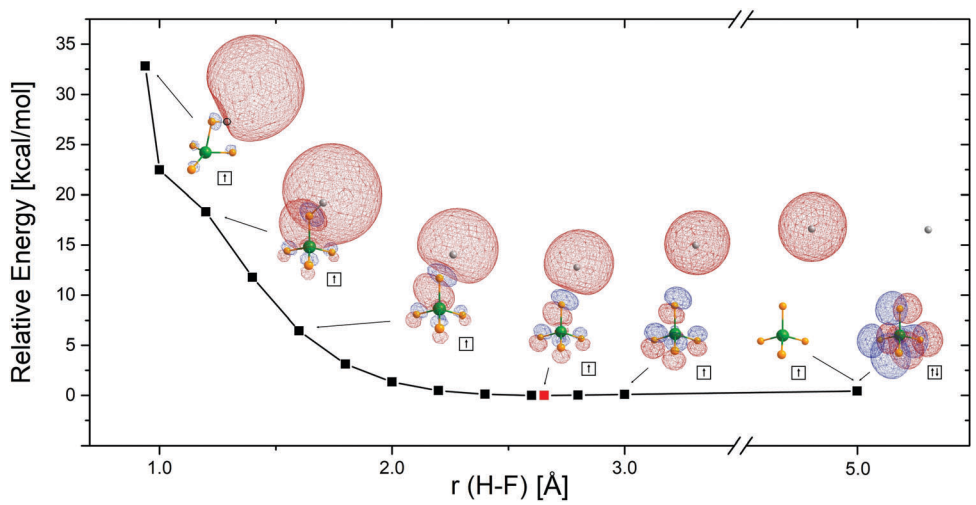

Fig. 1 The MP2/aug-cc-pVTZ + 4s4p3d energy profile for the $(HGaF_4)^-$ obtained by performing a relaxed scan of the ground doublet electronic state potential energy surface along the coordinate corresponding to the H–F distance. The molecular orbitals holding an excess electron are depicted for selected structures (for the structure corresponding to r(H–F) = 5.0 Å the highest doubly occupied orbital is also shown). The red data point indicates the shallow minimum at r(H–F) = 2.655 Å.

minimum on the ground anionic potential energy surface in the vicinity of the lowest energy structure of the neutral $HGaF_4$ molecule confirms that the $(HGaF_4)^-$ dipole-bound anion is indeed geometrically unstable and its structural reorganization proceeds promptly. The potential energy curve depicted in Fig. 1 is repulsive, hence the structure is expected to relax in this direction.

It is important to stress that the energy of the anion is always lower than that of the neutral along the fragmentation path (see the VDE values gathered in Table 1). Selected arbitrarily chosen structures and their corresponding SOMOs are presented on this relaxation path (for r(H–F) = 0.939, 1.200, 1.600, 2.655, 3.000, and 5.000 Å) whereas the detailed values characterizing the H–F distance, Ga–FH bond length, the F–Ga–F–F dihedral angle (in the GaF_3 fragment), and the relative energy for all data points shown are gathered in Table 1. The evolution of the SOMO orbital indicates that the unpaired electron penetrates the valence region while the anti-bonding H–F character escalates. Finally, for r(H–F) = 5.0 Å where both $(HGaF_4)^-$ and H might be considered separated, the unpaired electron that had been initially described by the dipole orbital can be thought of as assigned to the departing hydrogen atom; however, we would like to stress that such a description provides only a simplified explanation as it is based on the one electron approximation. In order to shed more light on this process, the following explanation might be offered: the process begins with attaching the excess electron to the equilibrium structure of the neutral $HGaF_4$ consisting of the F_3Ga and FH subunits linked *via* the Ga–F dative bond (this neutral species is in a singlet closed shell electronic state and its anion's lowest unoccupied molecular orbital is a dipole orbital having a negative energy eigenvalue). Hence, the excess electron is initially described by this dipole orbital, which leads to a doublet anionic state. It is important to emphasize that three electrons are crucial for describing the overall process, namely, the unpaired electron initially occupying the dipole orbital and the electron pair initially localized in the σ(F–H) bonding orbital of the HF subunit (the fourth Ga–F bond is not yet formed). As the r(H–F) distance increases, the SOMO is evolving but the system remains a doublet electronic state; however, the fourth Ga–F bond is being formed simultaneously and it contains two electrons and as the F–H bond breaks it generates a hydrogen atom that contains one electron. Thus, the singly occupied molecular orbital at the end of the process corresponds to the H atom 1s orbital, whereas the highest doubly occupied molecular orbital (depicted in Fig. 1 for the final r(H–F) distance of 5.0 Å) is distributed among the ligands in the $(GaF_4)^-$ anion. To summarize briefly, the three ''active'' electrons are localized in the following manner: at the beginning of the process – two electrons in a bonding σ(F–H) orbital and one electron in the dipole orbital; at the end of the process – two electrons in the bonding σ(Ga–F) orbital and one electron in the departing H atom 1s orbital. It is important to notice that both the initial and final dominant electronic configurations are of the same symmetry $(\sigma_1)^2(\sigma_2)^1$, thus we do not have two configurations that cross; instead, there is one dominant configuration whose two orbitals smoothly evolve (one from σ(F–H) to σ(Ga–F); the other from dipole orbital to the H atom 1s orbital).

As far as the structural reorganization is concerned, the described process progressively leads to the tetrahedral GaF_4 moiety. Indeed, the previously elongated Ga–FH bond shortens and the F–Ga–F–F dihedral angle in the GaF_3 subunit approaches 120° when the H–F distance increases, see Table 1. Then, the flat region of the anionic potential energy surface is reached (at r(H–F) of *ca.* 2.3 Å), yet the energy keeps decreasing slowly until the shallow minimum (whose depth does not exceed 1 kcal mol^{-1}) is achieved at r(H–F) = 2.655 Å (see the red data point in Fig. 1). Hence, our relaxed scan leads to the final system that corresponds to the $(GaF_4)^-$ and H fragments separated by the relatively large distance of 5.0 Å. Due to the fact that the minimum at r(H–F) = 2.655 Å is very shallow, the hydrogen atom detachment may further progress almost freely, as the energy cost of surmounting the kinetic barrier is extremely small (less than 1 kcal mol^{-1}, see Table 1). The confirmation of the nature of final fragmentation products is provided by the Merz–Singh–Kollman population analysis performed for the resulting $(GaF_4\cdots H)^-$ system having the stationary point characteristic. Namely, we found that the partial atomic charge of nearly zero (+0.002 a.u.) is localized on the H atom whereas the partial atomic charges localized on the Ga and F atoms sum up to *ca.* −1 a.u. (−0.998 a.u.). The localization of almost entire (99.9%) unpaired spin density on the distant H atom additionally supports our conclusion that the resulting $(GaF_4\cdots H)^-$ system consists of the $(GaF_4)^-$ closed-shell anion weakly interacting with the escaping hydrogen atom, hence the overall process should be described by the following scheme: $HGaF_4 + e \rightarrow (HGaF_4)^- \rightarrow H + (GaF_4)^-$.

3.3. The energy balance and duration of the fragmentation process

As already explained, excess electron attachment to the $HGaF_4$ molecule leads initially to the formation of $(HGaF_4)^-$ dipole bound anion and subsequently causes its fragmentation. Once the dipole-bound anionic state is formed, the excess electron is already bound to the molecular framework of $HGaF_4$ and thus might penetrate its valence region; however, the evolution of the excess electron density distribution has to be caused by some influential factor. According to our description, the possibility of formation of a very strongly bound anionic state is the thermodynamic driving force of this process. Namely, the $(GaF_4)^-$ superhalogen anion is the final product of the $(HGaF_4)^-$ reorganization, once the hydrogen atom is ejected. Indeed, as depicted in Fig. 1 (see the doubly occupied orbital for r(H–F) = 5.0 Å) and explained in the preceding section, one of the fragmentation products corresponds to the tetrahedral $(GaF_4)^-$ anion exhibiting large electronic stability.[53,54]

The analysis of the energy profile presented in Fig. 1 reveals that the whole $HGaF_4 + e \rightarrow (HGaF_4)^- \rightarrow H + (GaF_4)^-$ process is exoenergetic by 32.8 kcal mol^{-1}. We verified that this energy difference can be reproduced by summing up the energy effects related to the series of events occurring during the fragmentation reaction. Indeed, if one considers the following processes: (i) homolytical cleavage of the H–F bond (−143.7 kcal mol^{-1});

(ii) the Ga ← F dative bond rupture associated with the $FH\cdots FGaF_2$ hydrogen bond cleavage (−16.8 kcal mol^{-1}); (iii) excess electron attachment to the F atom (+83.9 kcal mol^{-1}); and (iv) formation of the valence bond upon the F^- attachment to GaF_3 (+109.7 kcal mol^{-1}), then the resulting value of 33.1 kcal mol^{-1} is achieved (positive and negative numbers correspond to energy gains and losses, respectively; all values are predicted at the theory level employed in this work to assure consistency). Since the value of 33.1 kcal mol^{-1} (obtained by summing up the energy effects associated to the processes mentioned) is very close to the energy difference (32.8 kcal mol^{-1}) from Table 1, we conclude that the $HGaF_4 + e \rightarrow (HGaF_4)^- \rightarrow H + (GaF_4)^-$ reaction may likely be thought of as consisting of such 'elementary' steps. Moreover, the observation that the overall energy effect associated to the excess electron driven superacid fragmentation could be successfully decomposed into such contributions (each of which might be independently estimated) seems to be useful for predicting the energy effect of the hitherto unknown processes induced by extra electron attachment to superacids.

The rate of the superacid fragmentation process can be estimated by calculating the time (t) it takes from the moment when the superacid molecule captures an excess electron until the moment when the hydrogen atom is detached from the remaining system. Since the potential energy curve for this process is known (see Fig. 1) then the 'starting point' (r_{start}) and the 'ending point' (r_{stop}) might be defined as corresponding to the initial excess electron attachment (r(H–F) = 0.939 Å in Fig. 1) and the point r(H–F) = 5.0 Å (see Fig. 1) at which the H atom is fully detached, respectively. Since the time dt it takes to move a small distance dr is given by $dt = \frac{dr}{\frac{dr}{dt}}$ and assuming that the system breaks apart into two sub-systems GaF_4 and H, the speed $\frac{dr}{dt}$ is given in terms of the GaF_4–H reduced mass μ by using

$$\frac{1}{2}\mu\left(\frac{dr}{dt}\right)^2 = [E - V(r)],$$

where $V(r)$ is the potential as a function of the coordinate r describing the GaF_4–H separation, and E is the initial energy where the "trajectory" starts (*i.e.*, at r_{start}). Hence, the total time it takes to begin at a point r_{start} and to move to a point r_{stop} is given by

$$t = \int_{r_{start}}^{r_{stop}} \frac{\sqrt{\mu}}{\sqrt{2[E - V(r)]}} dr$$

By using the above formula with the $V(r)$ potential presented in Fig. 1, we calculated the total time of the fragmentation process to be 1.51 × 10^{-14} s. Taking into account that a single H–F stretching vibration ($\nu_{(H-F)}$ = 3861 cm^{-1}, as calculated for the $HGaF_4$ molecule) takes 0.86 × 10^{-14} s, one may expect the fragmentation reaction to occur during approximately two such vibrational motions.

3.4. The possibility of electron autodetachment

Especially at geometries near that of the initially formed dipole-bound state, there exists the possibility that the loosely bound electron could be ejected through a process involving transfer of vibrational energy to electronic energy.[55,56] In particular, vibrational modes of the anion whose motions strongly modulate the magnitude of the dipole moment are expected to be most effective in inducing such autodetachment. At the geometry of the dipole-bound anion, we show in Table 2 the infrared (IR) intensities (which reflect the variations in magnitudes of the dipole moments) and vibrational frequencies for five modes having the largest intensities.

Table 2 Selected harmonic vibrational frequencies predicted for the $HGaF_4$ system at its equilibrium geometry

Frequency (symmetry)	IR intensity [km mol^{-1}]	Description
220 cm^{-1} (a')	105	GaF_3 inversion (umbrella)
433 cm^{-1} (a'')	157	Ga–F–H rocking
664 cm^{-1} (a')	183	Ga–F–H bending
751 cm^{-1} (a'')	124	Ga–F out-of-phase stretching
3861 cm^{-1} (a')	244	F–H stretching

Because the excess electron is bound by *ca.* 1451 cm^{-1}, one quantum of excitation of the F–H stretching mode would be expected to lead to vibration-to-electronic energy transfer induced electron ejection. On the other hand, excitation of any of the other vibrational modes would have to involve more than single excitation to effect electron ejection. However, as the anion's geometry evolves along the dissociation path illustrated in Fig. 1, the electron binding energy becomes large enough to render this energy-transfer mechanism much less likely to produce electron loss. So, the $(HGaF_4)^- \rightarrow H + (GaF_4)^-$ dissociation is expected to be attenuated by electron loss (i) if excess H–F vibrational energy is present but (ii) only briefly after the initial dipole-bound species is formed.

4. Conclusions

We studied excess electron attachment to the $HGaF_4$ superacid by employing *ab initio* quantum chemistry methods. The calculations performed with the CCSD(T) and MP2 methods and employing the aug-cc-pVTZ + 4s4p3d basis set led us to the following conclusions:

(i) Due to its polarity the $HGaF_4$ molecule can attract a distant excess electron and form a dipole-bound anionic state having a vertical electron attachment energy of 1451 cm^{-1}.

(ii) Geometrical instability of the $(HGaF_4)^-$ dipole-bound anion causes its structural reorganization driven by the formation of the more stable $(GaF_4)^-$ valence-bound superhalogen anion.

(iii) The $(HGaF_4)^- \rightarrow (GaF_4)^- + H$ fragmentation proceeds spontaneously and involves the simultaneous shortening of one Ga–F bond, forming a tetrahedral GaF_4 structure, hydrogen atom loss, and excess electron density migration.

(iv) The initially formed $(HGaF_4)^-$ dipole-bound anion, although only vertically electronically stable, plays an important role in the overall process as it enables a long range excess electron attraction and opens the door to the further reaction steps.

(v) The $HGaF_4 + e \rightarrow H + (GaF_4)^-$ reaction is exoergetic by 32.8 kcal mol^{-1} and this energy difference can be reproduced

by considering the energy effects related to the series of events occurring during the fragmentation reaction.

(vi) The total time of the fragmentation process considered was estimated to be *ca.* 1.51×10^{-14} s.

(vii) The described mechanism of dissociative electron attachment is expected to be general with respect to Lewis–Brønsted superacids having sufficient polarity.

Conflicts of interest

There are no conflicts to declare.

Acknowledgements

This research was supported by the Polish Ministry of Science and Higher Education grant no. DS 530-8375-D499-18 and partially by the Polish Ministry of Science and Higher Education grant no. BMN 538-8370-B732-17. The calculations have been carried out using resources provided by Wroclaw Centre for Networking and Supercomputing (http://wcss.pl) grant no. 350 (to M. C.).

References

1 R. A. Zubarev, N. L. Kelleher and F. W. McLafferty, *J. Am. Chem. Soc.*, 1998, **120**, 3265–3266.
2 E. A. Syrstad and F. Tureček, *J. Phys. Chem. A*, 2001, **105**, 11144–11155.
3 J. E. P. Syka, J. J. Coon, M. J. Schroeder, J. Shabanowitz and D. F. Hunt, *Proc. Natl. Acad. Sci. U. S. A.*, 2004, **101**, 9528–9533.
4 J. J. Coon, J. E. P. Syka, J. C. Schwartz, J. Shabanowitz and D. F. Hunt, *Int. J. Mass Spectrom.*, 2004, **236**, 33–42.
5 M. Czapla and P. Skurski, *Phys. Chem. Chem. Phys.*, 2015, **17**, 19194–19201.
6 M. Czapla and P. Skurski, *Chem. Phys. Lett.*, 2015, **630**, 1–5.
7 M. Czapla and P. Skurski, *J. Phys. Chem. A*, 2015, **119**, 12868–12875.
8 I. Anusiewicz, S. Freza and P. Skurski, *Polyhedron*, 2018, **144**, 125–130.
9 M. Czapla, I. Anusiewicz and P. Skurski, *Chem. Phys.*, 2016, **465–466**, 46–51.
10 M. Czapla and P. Skurski, *Int. J. Quantum Chem.*, 2018, **118**, e25494.
11 M. Czapla, I. Anusiewicz and P. Skurski, *RSC Adv.*, 2016, **6**, 29314–29325.
12 J. Brzeski, I. Anusiewicz and P. Skurski, *Theor. Chem. Acc.*, 2018, **137**, 57.
13 G. L. Gutsev and A. I. Boldyrev, *Chem. Phys.*, 1981, **56**, 277–283.
14 G. L. Gutsev, R. J. Bartlett, A. I. Boldyrev and J. Simons, *J. Chem. Phys.*, 1997, **107**, 3867–3875.
15 M. K. Scheller and L. S. Cederbaum, *J. Chem. Phys.*, 1994, **100**, 8934–8942.
16 J. V. Ortiz, *Chem. Phys. Lett.*, 1993, **214**, 467–472.
17 J. V. Ortiz, *J. Chem. Phys.*, 1993, **99**, 6727–6731.
18 G. L. Gutsev, P. Jena and R. J. Bartlett, *Chem. Phys. Lett.*, 1998, **292**, 289–294.
19 X.-B. Wang, C.-F. Ding, L.-S. Wang, A. I. Boldyrev and J. Simons, *J. Chem. Phys.*, 1999, **110**, 4763–4771.
20 S. Smuczyńska and P. Skurski, *Chem. Phys. Lett.*, 2007, **443**, 190–193.
21 S. Freza and P. Skurski, *Chem. Phys. Lett.*, 2010, **487**, 19–23.
22 S. Smuczyńska and P. Skurski, *Inorg. Chem.*, 2009, **48**, 10231–10238.
23 I. Anusiewicz, *J. Phys. Chem. A*, 2009, **113**, 6511–6516.
24 I. Anusiewicz, *J. Phys. Chem. A*, 2009, **113**, 11429–11434.
25 C. Sikorska, S. Freza, P. Skurski and I. Anusiewicz, *J. Phys. Chem. A*, 2011, **115**, 2077–2085.
26 B. Z. Child, S. Giri, S. Gronert and P. Jena, *Chem. – Eur. J.*, 2014, **20**, 4736–4745.
27 C. Sikorska and P. Skurski, *Chem. Phys. Lett.*, 2012, **536**, 34–38.
28 C. Sikorska and P. Skurski, *Inorg. Chem.*, 2011, **50**, 6384–6391.
29 R. A. Zubarev, N. A. Kruger, E. K. Fridriksson, M. A. Lewis, D. M. Horn, B. K. Carpenter and F. W. McLafferty, *J. Am. Chem. Soc.*, 1999, **121**, 2857–2862.
30 R. A. Zubarev, D. M. Horn, E. K. Fridriksson, N. L. Kelleher, N. A. Kruger, M. A. Lewis, B. K. Carpenter and F. W. McLafferty, *Anal. Chem.*, 2000, **72**, 563–573.
31 G. D. Purvis III and R. J. Bartlett, *J. Chem. Phys.*, 1982, **76**, 1910–1918.
32 J. A. Pople, M. Head-Gordon and K. Raghavachari, *J. Chem. Phys.*, 1987, **87**, 5968–5975.
33 R. A. Kendall, T. H. Dunning Jr. and R. J. Harrison, *J. Chem. Phys.*, 1992, **96**, 6796–6806.
34 P. Skurski, M. Gutowski and J. Simons, *Int. J. Quantum Chem.*, 2000, **80**, 1024–1038.
35 C. Sikorska, D. Ignatowska, S. Freza and P. Skurski, *J. Theor. Comput. Chem.*, 2011, **10**, 93–110.
36 M. W. Schmidt and K. Ruedenberg, *J. Chem. Phys.*, 1979, **71**, 3951–3962.
37 B. H. Besler, K. M. Merz Jr. and P. A. Kollman, *J. Comput. Chem.*, 1990, **11**, 431–439.
38 M. J. Frisch, *et al.*, *Gaussian 09, Revision D.01*, Gaussian, Inc., Wallingford CT, 2009.
39 C. Desfrançois, V. Périquet, S. Carles, J. P. Schermann and L. Adamowicz, *Chem. Phys.*, 1998, **239**, 475–483.
40 M. Gutowski and P. Skurski, *Recent Res. Dev. Phys. Chem.*, 1999, **3**, 245–260.
41 J. Simons and P. Skurski, in *Theoretical Prospects of NegativeIons*, ed. J. Kalcher, Research Signpost, Trivandrum, 2002.
42 K. D. Jordan and W. Luken, *J. Chem. Phys.*, 1976, **64**, 2760–2766.
43 K. D. Jordan and J. J. Wendoloski, *Chem. Phys.*, 1977, **21**, 145–154.
44 L. Adamowicz and E. A. McCullough Jr., *Chem. Phys. Lett.*, 1984, **107**, 72–76.
45 G. L. Gutsev and L. Adamowicz, *Chem. Phys. Lett.*, 1995, **246**, 245–250.
46 G. L. Gutsev, M. Nooijen and R. J. Bartlett, *Chem. Phys. Lett.*, 1997, **267**, 13–19.
47 M. Gutowski, K. D. Jordan and P. Skurski, *J. Phys. Chem. A*, 1998, **102**, 2624–2633.
48 P. Skurski, M. Gutowski and J. Simons, *J. Chem. Phys.*, 1999, **110**, 274–280.

49 J. Simons, *J. Phys. Chem. A*, 2008, **112**, 6401–6511.
50 P. Skurski, M. Gutowski and J. Simons, *J. Chem. Phys.*, 1999, **110**, 274–280.
51 P. Skurski, M. Gutowski and J. Simons, *J. Phys. Chem. A*, 1999, **103**, 625–631.
52 P. Skurski, M. Gutowski and J. Simons, *J. Chem. Phys.*, 2001, **114**, 7443–7449.
53 M. Gutowski, A. I. Boldyrev, J. V. Ortiz and J. Simons, *J. Am. Chem. Soc.*, 1994, **116**, 9262–9268.
54 X. Wang and L. Andrews, *J. Am. Chem. Soc.*, 2011, **133**, 3768–3771.
55 J. Simons, *J. Am. Chem. Soc.*, 1981, **103**, 3971–3976.
56 P. K. Acharya, Rick A. Kendall and J. Simons, *J. Am. Chem. Soc.*, 1984, **106**, 3402–3407.